Discovery Immunology, 2022, **1**, 1–11
https://doi.org/10.1093/discim/kyac002
Advance access publication 10 May 2022
Research Article

Research Article

NKG2D signaling regulates IL-17A-producing γδT cells in mice to promote cancer progression

Sophie Curio[1], Sarah C. Edwards[2,3], Toshiyasu Suzuki[2,3], Jenny McGovern[1], Chiara Triulzi[1], Nagisa Yoshida[1], Gustav Jonsson[1], Teresa Glauner[2,3], Damiano Rami[2,3], Robert Wiesheu[2,3], Anna Kilbey[2,3], Rachel Violet Purcell[4], Seth B. Coffelt[2,3,*] and Nadia Guerra[1,*]

[1]Department of Life Sciences, Imperial College London, London, UK
[2]Institute of Cancer Sciences, University of Glasgow, Glasgow, UK
[3]Cancer Research UK Beatson Institute, Glasgow, UK
[4]Department of Surgery, University of Otago, Christchurch, New Zealand

*Correspondence: Nadia Guerra, Imperial College London, SAF Building, South Kensington Campus, London SW7 2AZ, UK. Email: n.guerra@imperial.ac.uk; Seth B. Coffelt, Cancer Research UK Beatson Institute, Garscube Estate, Switchback Road, Glasgow G61 1BD, UK. Email: seth.coffelt@glasgow.ac.uk

Abstract

γδT cells are unconventional T cells particularly abundant in mucosal tissues that play an important role in tissue surveillance, homeostasis, and cancer. γδT cells recognize stressed cells or cancer cells through the NKG2D receptor to kill these cells and maintain normality. Contrary to the well-established anti-tumor function of these NKG2D-expressing γδT cells, we show here that, in mice, NKG2D regulates a population of pro-tumor γδT cells capable of producing IL-17A. Germline deletion of *Klrk1*, the gene encoding NKG2D, reduced the frequency of γδT cells in the tumor microenvironment and delayed tumor progression. We further show that blocking NKG2D reduced the capability of γδT cells to produce IL-17A in the pre-metastatic lung and that co-culture of lung T cells with NKG2D ligand-expressing tumor cells specifically increased the frequency of γδT cells. Together, these data support the hypothesis that, in a tumor microenvironment where NKG2D ligands are constitutively expressed, γδT cells accumulate in an NKG2D-dependent manner and drive tumor progression by secreting pro-inflammatory cytokines, such as IL-17A.

Graphical Abstract

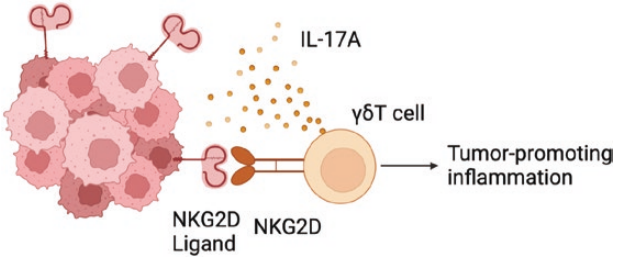

Keywords: NKG2D, γδT cells, inflammation, tumor immunology

Abbreviations: CAR: chimeric antigen receptor;FMO: fluorescence minus one;HCT: hematocrit;IEL: intestinal epithelial cells;LPL: lamina propria lymphocytes;MFI: mean fluorescence intensity;SI: small intestine;TIL: tumor-infiltrating lymphocytes;WT: wild-type

Introduction

Cancers affecting mucosal tissues, such as the intestine or the lung, present a global health burden, together making up more than 20% of deaths caused by cancer annually [1]. Mucosal tissues contain large numbers of unconventional lymphocytes, including γδT cells, which are involved in tissue surveillance and play an important role in the early response against infection and cancer [2, 3]. Indeed, mouse skin-resident γδT cells, activated by stress ligands through the receptor NKG2D, protect against chemically induced carcinogenesis [4, 5]. Nonetheless, other γδT-cell subsets can contribute to malignancies in certain contexts. Vγ4$^+$and Vγ6$^+$ γδT cells in the lung play a critical role in supporting pulmonary metastasis of p53-deficient mammary tumors through expression of IL-17A, and are activated by IL-1β derived from tumor-associated macrophages [6, 7]. In primary lung cancer, IL-17A-producing Vγ6$^+$ γδT cells promote tumorigenesis in a microbiota-dependent manner [8]. Germline deletion of *Tcrd*,

Received 12 January 2022; Revised 28 March 2022; Accepted for publication 20 April 2022

which results in the absence of γδT cells, ameliorates disease burden in models of intestinal cancer, indicating a pro-tumor role for γδT cells in intestinal malignancies [9, 10]. Yet, the molecular pathways and mucosal tissue environments leading to this pro-tumor role of γδT cells remain poorly understood.

NKG2D is a potent immunoreceptor expressed on various innate and adaptive immune cells including γδT cells [11–13]. Ligands for NKG2D are stress-induced molecules typically absent from healthy tissue [14]. Once triggered by one of its ligands, NKG2D elicits a strong immune response, resulting in the secretion of cytokines and cytotoxic molecules to induce target cell apoptosis. The presence of NKG2D ligands on a large variety of tumors identified the NKG2D/NKG2D ligand axis as an important player in anti-tumor immunity. This has been demonstrated in various *in vitro* killing assays and mouse models of cancer [14–16]. Its potent anti-tumor activity makes NKG2D a promising candidate for use in immunotherapy with several clinical trials exploring NKG2D as a potential chimeric antigen receptor (CAR), to specifically eliminate NKG2D ligand-expressing tumor cells [17–19]. In contrast with its anti-tumor effect, NKG2D can be deleterious in contributing to various inflammatory disorders, including inflammatory bowel diseases [20, 21] and allergic asthma [22]. In the context of inflammation-driven cancer, NKG2D-expressing cells can ultimately lead to cancer progression through their ability to sustain tissue inflammation and cause tissue damage. This was evidenced in a model of chemically induced hepatocellular carcinoma where NKG2D ligands are highly expressed in both tumor and non-tumor adjacent liver tissues [23, 24]. Whether this pro-tumor effect is limited to the liver tissue or associated with other cancer types driven by inflammation remains to be demonstrated.

In this study, we investigated the function of IL-17A-producing γδT cells that co-express NKG2D in mice. We found that intestinal tumor progression is delayed in both γδT cell- and NKG2D-deficient mice. NKG2D deficiency was associated with a marked reduction of γδT cells in the tumor microenvironment and NKG2D-expressing γδT cells displayed an increased ability to produce IL-17A in diseased mice. Furthermore, in the pre-metastatic lung of a mammary tumor model, blocking NKG2D reduced IL-17A production, extending our observation to an additional mucosal site. Lastly, we demonstrate that lung γδT cells expand in an NKG2D-dependent manner *in vitro* in line with their enrichment in a tumor microenvironment which harbor large amounts of NKG2D ligands. Together, these findings uncover a new role for the NKG2D receptor on pro-tumor γδT cells during cancer progression that highlight the functional diversity of this receptor.

Results

γδT cells express NKG2D, produce IL-17, and contribute to intestinal tumor progression

We investigated the function of γδT cells in intestinal cancer testing the hypothesis that these cells contribute to tumor progression in an NKG2D-dependent manner by creating an inflammatory, tumor-promoting environment. We employed a cancer model driven by the complete loss of the *Apc* gene specifically in intestinal epithelial cells (IEL): the *Villin-Cre^{ERT2};Apc$^{F/+}$* model. Similar to patients with mutations in the tumor suppressor *APC* gene, these mice are predisposed to intestinal adenoma formation. We crossed *Villin-Cre^{ERT2};Apc$^{F/+}$* mice with mice carrying a germline deletion of the *Tcrd* gene, resulting in the complete loss of γδT cells (*Villin-Cre^{ERT2};Apc$^{F/+}$;Tcrd$^{-/-}$*). Tumor-bearing mice lacking γδT cells survived longer than control mice (Fig. 1a), demonstrating a pro-tumorigenic role for γδT cells in the development of *Apc*-deficient intestinal tumors. In this model, γδT cells increased expression of IL-17A (Fig. 1b) – a cytokine that promotes disease progression in human patients [25] – suggesting that IL-17A-producing γδT cells drive disease progression in this model.

Previous studies investigating the function of γδT cells in intestinal tumorigenesis have shown a disease-promoting role for γδT cells in the *Apc$^{min/+}$* mouse [9, 10], which harbor a point mutation in the *Apc* gene and present with a similar phenotype as the *Villin-Cre^{ERT2};Apc$^{F/+}$* mice. In the *Apc$^{min/+}$* mouse model, we determined the frequencies of NKG2D$^+$ γδT cells within the tumor microenvironment compared with healthy tissue. We found that NKG2D$^+$ γδT cells were increased more than 8-fold among tumor-infiltrating lymphocytes (TIL) compared with intestinal epithelial cells (IEL) and more than 2-fold when comparing to lamina propria lymphocytes (LPL) of healthy control mice (Fig. 1c). In addition to a change in frequencies, we found an increase in the mean fluorescence intensity (MFI) of NKG2D on γδT cells present in the tumor microenvironment of *Apc$^{min/+}$* mice compared to healthy tissue (Fig. 1c, middle and right), in line with previous studies [9]. Next, we profiled the NKG2D$^+$ γδT-cell population located in the draining mesenteric lymph nodes of tumor-bearing mice for cytokine production and found that they preferentially produced IL-17A over IFNγ (Fig. 1d). These data corroborated previous results showing that IL-17-producing γδT cells in the lung and axillary lymph nodes express the NKG2D receptor [26]. We questioned whether NKG2D ligands, which are constitutively expressed on healthy human intestinal epithelium [27], are present on tumors of *Apc$^{min/+}$* mice by measuring the expression of the mouse ligand, RAE-1. We confirmed that RAE-1 is expressed in the intestine of age-matched healthy control mice, and we found that RAE-1 is present at significant levels in tumors as well as tumor-surrounding tissue of *Apc$^{min/+}$*mice (Fig. 1e and f). Taken together, the increased frequency of NKG2D$^+$ γδT cells within the tumor microenvironment and the presence of NKG2D ligands suggest that NKG2D$^+$ γδT cells contribute to the immune response in *Apc$^{min/+}$* mice.

NKG2D promotes intestinal cancer progression

To study the function of NKG2D (encoded by the *Klrk1* gene) in the development of intestinal tumors, *Apc$^{min/+}$* mice were intercrossed with *Klrk1$^{+/-}$* mice to generate NKG2D-sufficient (*Apc$^{min/+}$;Klrk1$^{+/+}$*) and NKG2D-deficient (*Apc$^{min/+}$;Klrk1$^{-/-}$*) mice that were assessed for survival and tumor burden. *Apc$^{min/+}$;Klrk1$^{-/-}$* mice displayed significantly increased survival compared to *Apc$^{min/+}$;Klrk1$^{+/+}$* littermates (Fig. 2a), a delay in development of small intestinal tumors (Fig. 2b), as well as a 2-fold decrease in colonic tumors at disease endpoint (Fig. 2c). Hematocrit (HCT) was measured as an additional read out of disease severity. Anemia is a direct consequence of the high numbers of multiple polyps in the small intestine (SI), which can exceed 100 tumors per mouse, leading to significant blood loss. Blood collected at disease endpoint showed lower HCT levels in *Apc$^{min/+}$;Klrk1$^{+/+}$*mice compared

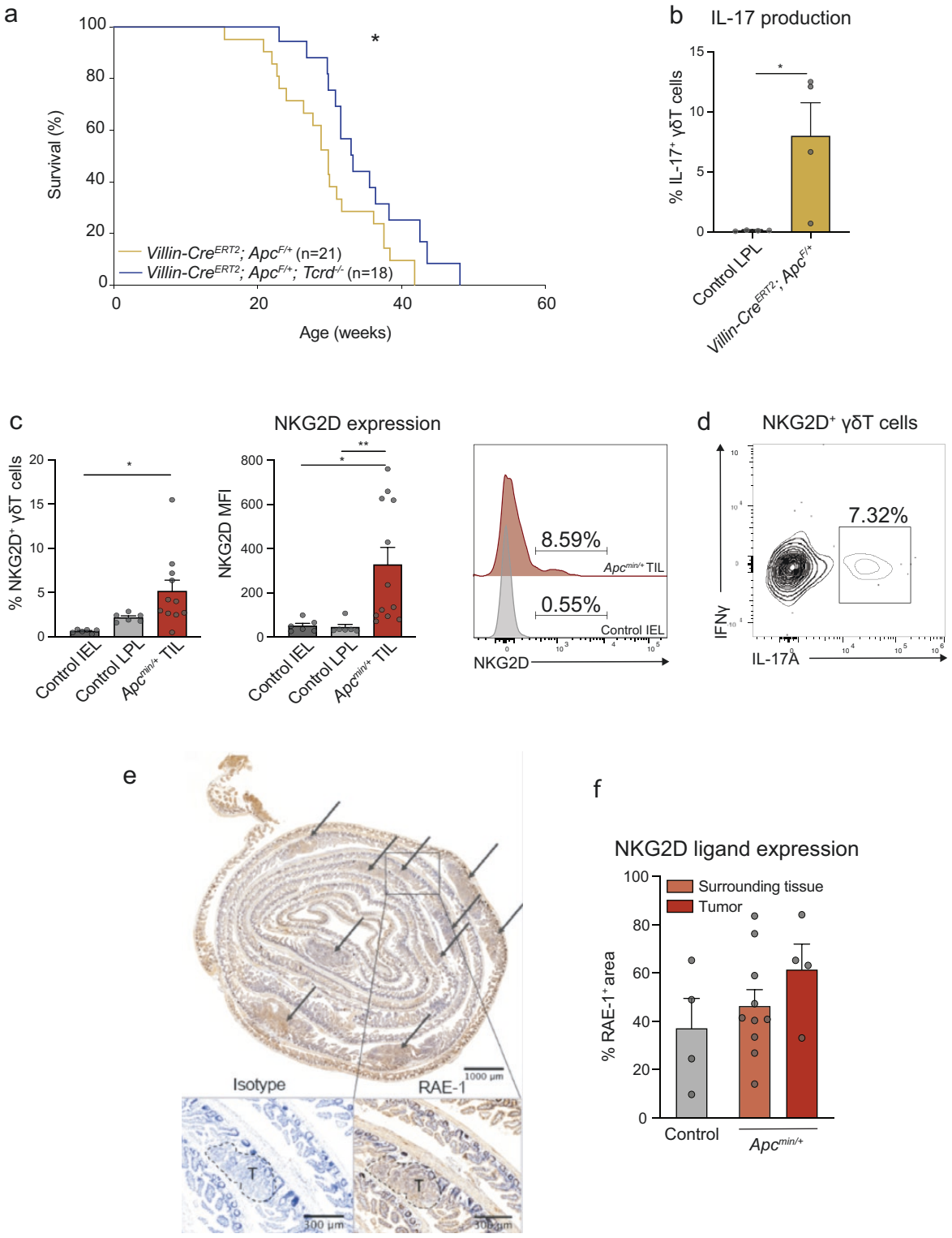

Figure 1: Tumor-infiltrating γδT cells express NKG2D and IL-17 and contribute to tumor progression. (a) Survival of *Villin-Cre*^{ERT2}*;Apc*$^{F/+}$(n=21) compared to γδT cell-deficient *Villin-Cre*^{ERT2}*; Apc*$^{F/+}$*;Tcrd*$^{-/-}$ (n=18) mice. (b) Frequencies of IL-17A producing T cells (gated on $CD3^+CD4^-CD8^-\gamma\delta TCR^+$) in the intestine of tumor-bearing *Villin-Cre*^{ERT2}*;Apc*$^{F/+}$ mice and tumor-free, wild-type mice ($n = 4$). (c) Frequencies (left), MFI (middle), and representative histograms (right) of NKG2D-expressing γδT cells in the healthy SI IEL and LPL ($n = 6$) from naïve mice compared to TIL isolated from SI tumors of *Apc*$^{min/+}$mice ($n = 8$-15) at 18–20 weeks. (d) Representative flow cytometry dot plot depicting IL-17A and IFNγ production by $NKG2D^+$ γδT cells isolated from the MLN of *Apc*$^{min/+}$ mice. (e) Representative image of RAE-1 staining in the small intestine of *Apc*$^{min/+}$mice including the unstained isotype control and (f) quantification of $RAE\text{-}1^+$ area in wild-type control mice ($n = 4$) compared to tissue surrounding the tumor ($n = 10$) and the tumor ($n = 4$) of *Apc*$^{min/+}$ mice determined by immunohistochemistry. T: tumor; SI: small intestine; LPL: lamina propria lymphocytes; IEL: intraepithelial lymphocytes; MLN: mesenteric lymph node. Bars represent mean ± SEM. Data points represent individual mice. Significance was determined using log-rank (Mantel–Cox) test (a), Mann–Whitney *U* or unpaired *t*-test following Shapiro–Wilk normality test (b), Kruksal–Wallis and Dunn's multiple comparison test (c, f). $*P \leq 0.05$.

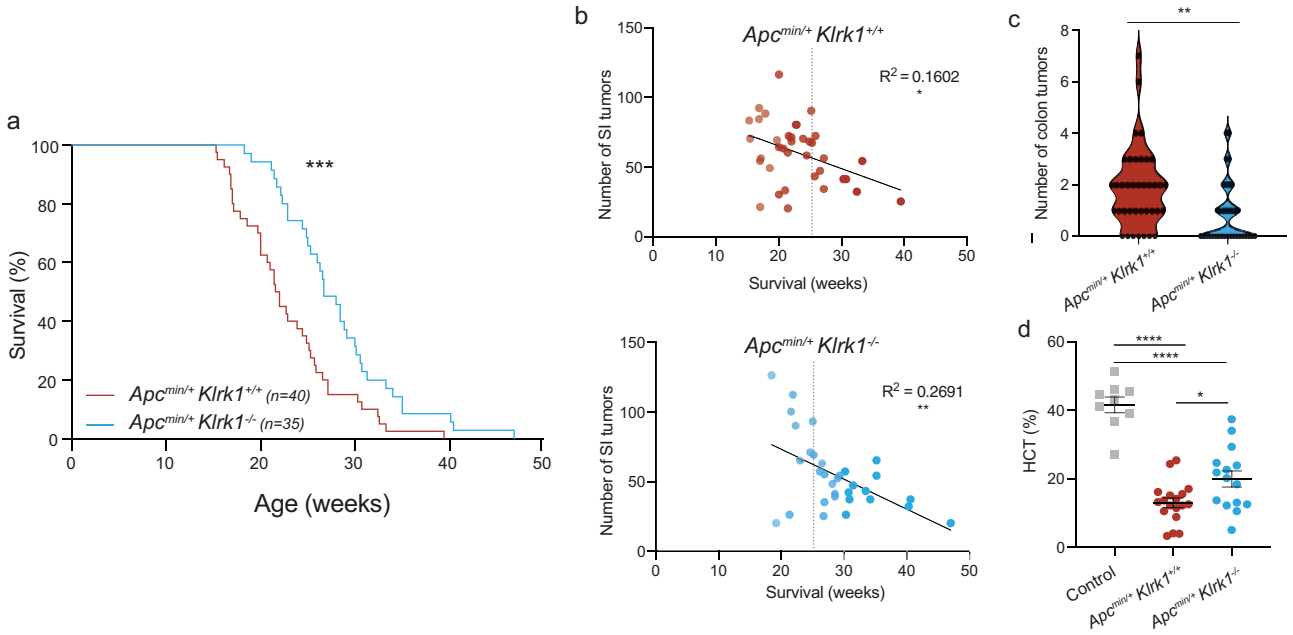

Figure 2: NKG2D expression drives disease severity. (a) Kaplan–Meier survival analysis of *Apc*$^{min/+}$;*Klrk1*$^{+/+}$ (n = 40) and *Apc*$^{min/+}$;*Klrk1*$^{-/-}$ (n = 35) mice. (b) Correlation between number of small intestinal (SI) tumors and survival in *Apc*$^{min/+}$;*Klrk1*$^{+/+}$ (top, red) and *Apc*$^{min/+}$;*Klrk1*$^{-/-}$ (bottom, blue) mice. (c) Number of tumors in the colon of *Apc*$^{min/+}$;*Klrk1*$^{+/+}$ (n = 40) and *Apc*$^{min/+}$;*Klrk1*$^{-/-}$ mice (n = 35) at disease endpoint. (d) Hematocrit (HCT) measures from the blood of healthy *Klrk1*$^{+/+}$ control mice (n = 8), *Apc*$^{min/+}$;*Klrk1*$^{+/+}$ (n = 18) and *Apc*$^{min/+}$;*Klrk1*$^{-/-}$ (n = 15) mice at disease endpoint. Data points represent individual mice. SI: small intestine; HCT: hematocrit. Significance was determined using log-rank (Mantel–Cox) test (a), linear regression (b), Mann–Whitney U or unpaired t-test following Shapiro–Wilk normality test (c) and one-way analysis of variance (ANOVA) and Tukey's multiple comparison test (d). *$P \leq 0.05$, **$P \leq 0.01$, ***$P \leq 0.001$, and ****$P \leq 0.0001$.

to *Apc*$^{min/+}$;*Klrk1*$^{-/-}$ mice (Fig. 2d), further supporting the observations that tumor progression is enhanced in the presence of NKG2D. Collectively, these data show that the predominant role of NKG2D in *Apc*-mutated models of intestinal tumorigenesis is contributing to a tumor-promoting response.

NKG2D regulates γδT cells in intestinal tumors

The high amount of NKG2D expressed by intestinal tumor-infiltrating γδT cells (Fig. 1c) prompted further investigations of their phenotype and function in this model. We found that γδT cells were more abundant in the tumor microenvironment of *Apc*$^{min/+}$;*Klrk1*$^{+/+}$ compared to *Apc*$^{min/+}$;*Klrk1*$^{-/-}$ mice (Fig. 3a and b). We then determined which γδT-cell subset was affected by the lack of NKG2D in tumor-bearing mice. We used the co-stimulatory molecule, CD27, to discriminate between CD27^{-} IL-17A-producing γδT cells and CD27^{+} IFNγ-producing γδT cells and investigate whether the ratio of these two populations was altered after deletion of NKG2D. This analysis showed a modest reduction of CD27^{-} γδT cells frequency in the absence of NKG2D (Supplementary Fig. 1a), prompting a deeper examination of this subset. Recent in-depth analysis of γδT-cell subsets has revealed that IL-17A-producing Vγ6 cells express high levels of PD-1 and lack of CD27 [26, 28, 29]. Accordingly, we observed that, in the lung, PD-1 is constitutively expressed on Vγ6^{+} cells and PD-1 expression by Vγ6^{+} cells is unchanged in NKG2D-deficient mice (Supplementary Fig. 1). Therefore, the frequency of PD-1^{+} γδT cells – as a surrogate marker for IL-17A-producing Vγ6 cells – was measured at 18–20 weeks and disease endpoint. Tumor-infiltrating PD-1^{+} γδT cells were increased 8-fold from early- to end-stage tumors in *Apc*$^{min/+}$;*Klrk1*$^{+/+}$ mice (Fig. 3c and d), indicating that Vγ6^{+} cells are enriched in intestinal tumors. However, this increase in PD-1^{+} γδT cells was blunted in tumors from NKG2D-deficient mice at disease endpoint (Fig. 3c and d). These data underscore the importance of NKG2D on IL-17A-producing Vγ6 cells during cancer progression, showing that accumulation of PD-1^{+} γδT cells in the tumor microenvironment of *Apc*$^{min/+}$;*Klrk1*$^{+/+}$ mice is at least in part regulated by NKG2D signaling.

IL-17A is a pro-inflammatory cytokine known to drive intestinal tumorigenesis in the *Apc*$^{min/+}$ mouse model and other colon cancer mouse models, where it is produced by γδT cells and CD4^{+} T cells [10, 30]. Therefore, we determined the frequencies of IL-17A-producing cells infiltrating intestinal tumors and found that the proportions of IL-17A-producing CD4^{+} T cells, CD8^{+} T cells and γδT cells were higher at disease endpoint than at 18–20 weeks of age (Fig. 3e). These populations were similarly represented in NKG2D-deficient and -sufficient mice (Fig. 3f). Nonetheless, we presumed that the cumulative amount of IL-17A being produced in the tumor microenvironment of NKG2D-deficient mice is reduced as a consequence of the reduced accumulation of γδT cells observed in these mice compared to the wild-type littermates (Fig. 3b). This conclusion is supported by the fact that the amount of IL-17A (i.e. fluorescence intensity) produced by NKG2D^{+} γδT cells localized in the MLN of tumor bearing, but not healthy mice, was higher than the amount produced by NKG2D– γδT cells (Fig. 3g). Together, these data indicate that NKG2D signaling regulates both the accumulation of PD-1^{+} γδT cells into tumors and their ability to produce IL-17A.

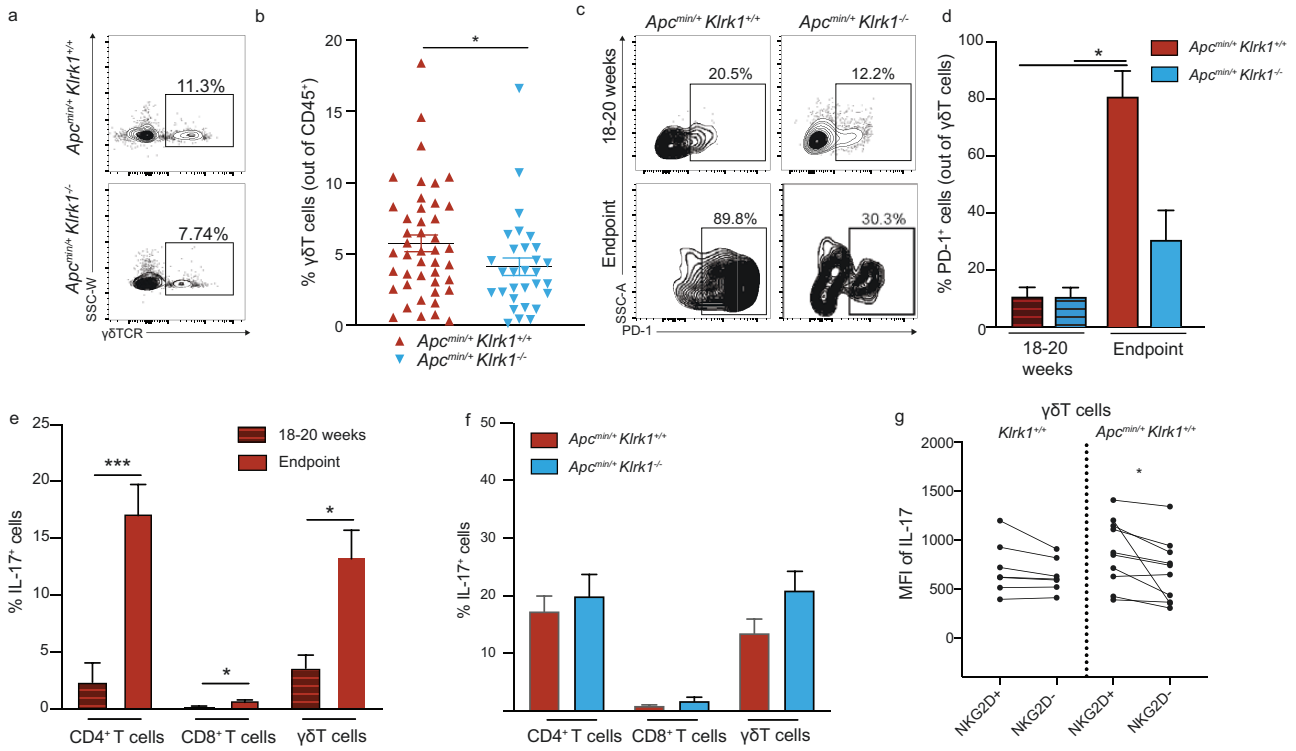

Figure 3: NKG2D regulates γδT cell accumulation and IL-17A expression in intestinal tumors. (a) Representative flow cytometry dot plots depicting γδT cells, gated on live CD3+ lymphocytes in the SI TME of *Apc*$^{min/+}$;*Klrk1*$^{+/+}$ (top) and *Apc*$^{min/+}$;*Klrk1*$^{-/-}$ mice (bottom) at disease endpoint. (b) Average frequencies of γδT cells at disease endpoint in *Apc*$^{min/+}$;*Klrk1*$^{+/+}$ (n = 44) compared to *Apc*$^{min/+}$;*Klrk1*$^{-/-}$ (n = 30) mice. Data points represent individual mice. (c) Representative flow cytometry dot plots depicting PD-1 expression on γδT cells in the SI TME of *Apc*$^{min/+}$;*Klrk1*$^{+/+}$ (left) and *Apc*$^{min/+}$;*Klrk1*$^{-/-}$ mice (right) at 18–20 weeks (top) and disease endpoint (bottom). (d) Average frequencies of PD-1 expressing γδT cells in the SI TME of *Apc*$^{min/+}$;*Klrk1*$^{+/+}$ and *Apc*$^{min/+}$;*Klrk1*$^{-/-}$ mice at 18-20 weeks (n = 11) compared to endpoint (n = 3–4). (e) Average frequencies of IL-17A+ T cells in the SI TME of *Apc*$^{min/+}$;*Klrk1*$^{+/+}$ mice at 18–20 weeks (n = 4–7) compared to endpoint (n = 22–24). (f) Average frequencies of IL-17A+ T cells in the SI TME of *Apc*$^{min/+}$;*Klrk1*$^{+/+}$ (n = 22–24) compared to *Apc*$^{min/+}$;*Klrk1*$^{-/-}$ (n = 17) mice at disease endpoint. (g) Direct comparison of IL-17A MFI in NKG2D+ and NKG2D- γδT cells, gated on live CD3+ lymphocytes, isolated from the MLN of *Klrk1*$^{+/+}$ (n = 6) and *Apc*$^{min/+}$;*Klrk1*$^{+/+}$ mice at 18–20 weeks (n = 10). SI: small intestine; TME: tumor microenvironment; MFI: mean fluorescence intensity; MLN: mesenteric lymph nodes. Bars represent mean ± SEM. Significance was determined using Mann–Whitney *U* or unpaired *t*-test following Shapiro–Wilk normality test (b, e, and f) or Kruksal–Wallis and Dunn's multiple comparison test (d) and paired *t*-test (g). *$P \leq 0.05$, **$P \leq 0.01$, ***$P \leq 0.001$.

NKG2D signaling stimulates pro-tumorigenic IL-17A-producing γδT cells

To further probe the role of NKG2D in mucosal IL-17+ γδT cells, we used a mammary tumor model where IL-17A-producing γδT cells drive lung metastasis [6, 7]. In these models, WNT-dependent activation of innate inflammation in response to mammary tumors leads to the production of IL-17 by lung resident-γδT cells [6, 7]. Thus, mammary tumor models represent a good system to interrogate the phenotype and function of IL-17A-producing γδT cells in the lung. As such, mice were transplanted with *K14-Cre;Brca1*$^{F/F}$*;Trp53*$^{F/F}$(KB1P) mammary tumor fragments [31] to activate lung IL-17A-producing γδT cells. We measured the expression of NKG2D by IL-17A-producing γδT cells (identified by the lack of CD27 expression) in tumor-bearing KB1P mice and tumor-free mice to determine whether tumors affect NKG2D expression on these cells. This comparison revealed that NKG2D expression remains constant between lung CD27- γδT cells in tumor-bearing KB1P mice and tumor-free mice (Fig. 4a). We then questioned whether NKG2D signaling could impact IL-17A expression by lung γδT cells. KB1P tumor-bearing mice were treated with IgG control antibodies or anti-NKG2D blocking antibodies and cytokine expression by lung γδT cells was measured. Blocking NKG2D resulted in reduced IL-17A expression in γδT cells when compared with controls (Fig. 4b and c), indicating that NKG2D signaling positively regulates pro-metastatic IL-17A-producing γδT cells in the lung. It is worth noting that, in addition to a reduction of IL-17A expression in γδT cells, we observed a reduction of IL-17A+ CD4+ T cells and Granzyme B+ NK cells after blockade with anti-NKG2D blocking antibodies (Supplementary Fig. 2).

To gain further insight into the regulation of γδT cells by NKG2D, we performed co-culture experiments where CD3+ T cells from the lungs of naïve mice were incubated with the NKG2D ligand (RAE-1)-expressing lymphoma cell line, YAC-1. In this assay, the proportion of γδT cells increased after interaction with YAC-1 cells (Fig. 4d and e, top). This was specifically due to an increase in CD27– γδT cells, which are capable of producing IL-17A (Fig. 4d and e, bottom). To show that this increase in CD27– γδT cells by RAE-1-expressing YAC-1 cells was directly dependent on NKG2D signaling, we generated mice whose IL-17A-producing γδT cells lack NKG2D expression. We crossed *Rorc-Cre* mice with *Klrk1*$^{F/F}$ mice so that activation of RORγt, the master transcription factor of the *Il17a* gene, deletes *Klrk1* by Cre recombinase. Lung CD3+ T cells from *Rorc-Cre;Klrk1*$^{F/F}$ mice were then co-cultured with RAE-1-expressing YAC-1 cells. However, in contrast with NKG2D-proficient γδT cells

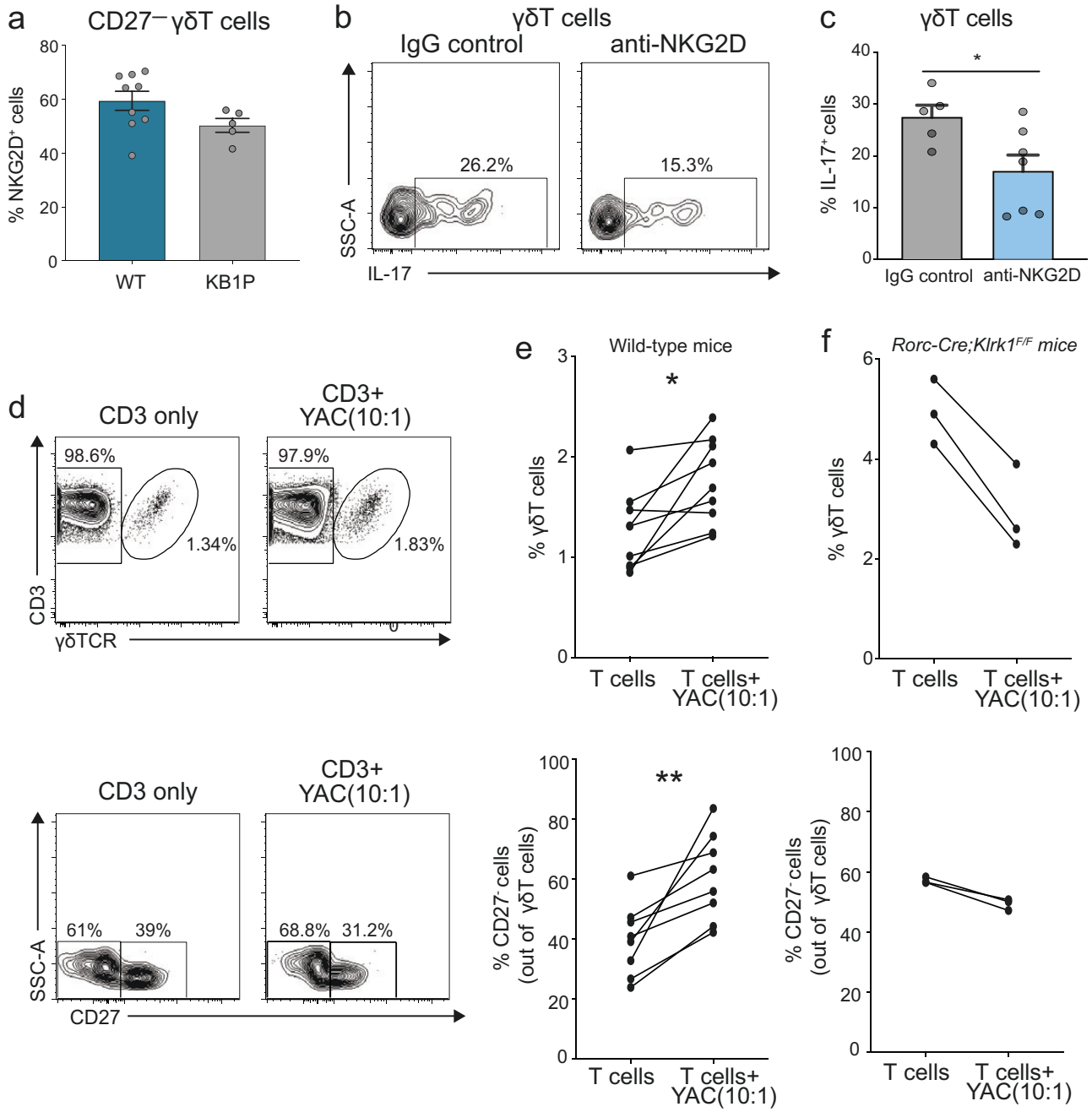

Figure 4: NKG2D signaling regulates IL-17A-producing T cells. (a) Average frequencies of NKG2D-expressing CD27⁻ γδT cells in the healthy lung of wild-type mice ($n = 9$) compared to the lung of KB1P tumor-bearing mice ($n = 5$). (b) Representative flow cytometry contour plots depicting IL-17A staining on γδT cells in mice bearing KB1P tumor transplants treated with isotype control IgG antibody or anti-NKG2D antibody. (c) Average frequencies of IL-17A-producing γδT cells, gated on live γδTCR⁺CD3⁺ T cells in mice bearing KB1P tumor transplants treated with the isotype control IgG ($n = 5$) antibody or anti-NKG2D ($n = 7$) antibody. (d) Representative flow cytometry dot plots of γδTCR (top, gated on CD3⁺ live lymphocytes) and CD27 expression (bottom, gated on γδTCR⁺CD3⁺ live lymphocytes) before and after co-culture of T cells isolated from the lung with NKG2D ligand-expressing YAC-1 cells. (e) Average frequencies of γδT cells (top) and CD27⁻ γδT cells (bottom) isolated from wild-type mice before and after co-culture of T cells isolated from the lung with YAC cells ($n = 8$). Each line represents one individual mouse. (f) Frequencies of *Rorc-Cre;Klrk1*$^{F/F}$ γδT cells (top) and CD27⁻ γδT cells (bottom) before and after co-culture of T cells isolated from the lung with YAC cells ($n = 3$). Each line represents one individual mouse. Bars represent mean ± SEM. Significance was determined using Mann–Whitney *U* or unpaired *t*-test following Shapiro–Wilk normality test (d) or paired *t*-test (f,g). $^*P \leq 0.05$, $^{**}P \leq 0.01$.

(Fig. 4e), the proportions of γδT cells and NKG2D-deficient *Rorc-Cre;Klrk1*$^{F/F}$ CD27– γδT cells failed to increase after co-culture with YAC-1 cells (Fig. 4f). These data demonstrate that lung NKG2D⁺CD27⁻ γδT cells selectively expand when cultured with RAE-1-expressing YAC-1 cells. Collectively, these data indicate that NKG2D signaling enhances activation of γδT cells, which are a source of pro-inflammatory IL-17A and contribute to tumor progression.

Discussion

The role of γδT cells in cancer is highly context dependent and specific subsets of γδT cells can either favor or inhibit tumorigenesis depending on the tissue and the local immune environment. How are γδT cells regulated and what tissue environments favor a tumor-promoting role is poorly understood. In this study, we report that γδT cells contribute to the development and progression of mucosal tumors in an NKG2D-dependent manner. Using a mouse model of intestinal cancer, we demonstrate that γδT cells drive tumor development and disease progression in mucosal tissue. We further show that NKG2D is essential for the accumulation of γδT cells in the tumor microenvironment and the production of IL-17A. Disease progression in *Klrk1*$^{-/-}$ mice is delayed and associated with lower tumor burden, which is contrary to the well-studied anti-tumor function of NKG2D [14–16]. We confirm the functional link between NKG2D and IL-17A by showing that antibody-mediated blocking of NKG2D specifically reduces the frequency of IL-17A-producing γδT cells in the lung. Co-culture of T cells isolated from the lung with NKG2D ligand-expressing tumor cells specifically increases the frequency of γδT cells, suggesting that the NKG2D/NKG2D ligand axis is involved in the accumulation of γδT cells in the tumor microenvironment. This is in line with previous studies showing NKG2D ligand-dependent recruitment and retention of NKG2D-expressing lymphocytes in the pancreas [32]. These conclusions support the idea that a tissue environment in which high levels of NKG2D ligand are expressed favors the accumulation of NKG2D^{+} cells. Whether the accumulation of NKG2D-expressing γδT cells in the tumor microenvironment of *Apc*$^{min/+}$ mice is the result of recruitment, enhanced retention, or local proliferation of NKG2D-expressing was not addressed in this study.

We show that RAE-1 expression is localized to the villi – not the crypt regions – within normal intestinal tissue and its expression is maintained in tumor tissue. This indicates that tumor progression was not a consequence of NKG2D ligand downregulation or shedding from tumors as reported in various cancer type but rather associated with its sustained expression. Clinical studies support our findings in showing a poor prognosis for CRC patients exhibiting MICA expression [33]. NKG2D has numerous ligands, including MULT-1 and H60 in mice as well as MICA, MICB, and ULBP family members in humans, which may differentially regulate NKG2D-expressing cells. Colorectal tumors express several NKG2D ligands; however, their level varies considerably and there is no consistent evidence of their prognostic value [34, 35]. NKG2D ligands can be post-translationally processed and proteolytically cleaved from the cell surface, which can affect NKG2D function [36, 37]. Future studies should, therefore, address how different NKG2D ligands regulate NKG2D-expressing γδT cells.

Our findings reveal a new molecular pathway of γδT cell-mediated tumor progression: while γδT cells have the potential to recognize tumor cells and initiate an anti-tumor response through the engagement of NKG2D, we provide further evidence for a pro-tumorigenic role in inflammation-driven mucosa-associated cancers. Specifically, we suggest that a subset of γδT cells expressing PD-1, a marker associated with IL-17A-producing Vγ6 cells [28], accumulate in the tumor microenvironment in an NKG2D-dependent manner. Nonetheless, other cell subsets are likely to be functionally involved in controlling tumor growth, e.g. IFNγ-producing γδT cells are present in the tumor that may contribute to an anti-tumor response. Similarly, NKG2D expression on other cell types, such as NK cells, may be beneficial and induce tumor cell lysis, in particular at early stages of disease.

IL-17A is a cytokine associated with colorectal cancer progression in humans [38, 39] and mice [8, 10]. A direct link between NKG2D and IL-17A was recently evidenced when Babic *et al.*, showed that NKG2D regulates T_H17 effector cell function and that lack of NKG2D on T cells ameliorates IL-17A-driven pathology [40]. In the context of tumor immunity, antibody blockade of NKG2D has previously been shown to partially reduce IL-17A production by γδT cells [41, 42]. These findings underline the need to better understand the function of tumor-infiltrating γδT cells and NKG2D-expressing immune cells, in light of recent clinical studies using γδT cell- and NKG2D-based approaches in immunotherapy [43–45]. While engagement of NKG2D can potentially lead to tumor regression by unleashing an anti-tumor immune response, we show that expression of NKG2D and its ligands in mucosal cancers can activate tumor-promoting immune subsets, such as IL-17A-producing γδT cells. We have previously shown that NKG2D-expressing CD8^{+} T cells associate with tumor growth in a model of liver cancer [23]. Here, we extend these findings of a pro-tumor effect for NKG2D to intestinal cancer and lung metastasis, and show that disease progression is mediated through distinct mechanisms.

Current studies using anti-NKG2D antibodies to treat Crohn's disease patients [46] and ongoing trials on NKG2D CAR-T cells in colorectal cancer patients will provide crucial information on the function of NKG2D in the context of intestinal inflammation and cancer. Together, we unravel a novel role for NKG2D-expressing γδT cells in mucosal immunity and tumorigenesis and uncover a paradoxical role of these cells during cancer development. Our data highlight the need to better understand the function of NKG2D^{+} γδT cells and NKG2D ligand expression in the tumor microenvironment, including tissue-specific immune responses.

Methods

Mice

Klrk1$^{+/-}$ heterozygous mice (*Klrk1*^{tm1Dhr}) [15] were crossed with *Apc*$^{min/+}$ mice to generate *Klrk1*$^{+/+}$;*Apc*$^{min/+}$, *Klrk1*$^{-/-}$;*Apc*$^{min/+}$, *Klrk1*$^{+/+}$;*Apc*$^{+/+}$ and *Klrk1*$^{-/-}$;*Apc*$^{+/+}$ mice. These mice were maintained on the C57BL/6J background. Studies on the lung were performed on *Klrk1*$^{-/-}$ mice (*Klrk1*$^{tm1.1Bpol}$) provided by Adrian Hayday (Francis Crick Institute, London) and maintained on the FVB/nJ background. *Villin-Cre*^{ERT2};*Apc*$^{F/+}$;*Tcrd*$^{-/-}$ mice were generated by crossing *Villin-Cre*^{ERT2};*Apc*$^{F/+}$ mice with *Tcrd*$^{-/-}$ mice. The alleles used were as follows: *Villin-Cre*^{ERT2}, *Apc*^{F} [47, 48], and *Tcrd*$^{-/-}$ [49]. *Villin-Cre*^{ERT2} experiments were performed on a mixed background (N8 for C57BL/6J). Recombination by *Villin-Cre*^{ERT2} was induced with one intraperitoneal (i.p.) injection of 80 mg/kg tamoxifen when mice reached 20 g. The health status of *Apc*$^{min/+}$ and *Villin-Cre*^{ERT2};*Apc*$^{F/+}$mice was checked and evaluated frequently. Disease severity was assessed using a scoring scheme that included parameters such as appearance, natural behavior, provoked behavior, body condition, and tumor score. For hematocrit (HCT) measurement, blood was collected from the tail vein of live mice into Eppendorf tubes

containing 100 µl of 0.5 M EDTA to prevent clotting. Blood parameters, including hematocrit. were measured using the XN-350 (Sysmex). Mice were humanely euthanized when they had reached the experimental endpoint.

Klrk1$^{F/F}$ mice were provided by Bojan Polic (University of Rijeka School of Medicine, Croatia) and crossed with *Rorc-Cre* mice (*Tg(Rorc-cre)1Litt*) to generate *Rorc-Cre;Klrk1*$^{F/F}$ mice. Mice were backcrossed to FVB/nJ background to N10.

K14-Cre;Brca1$^{F/F}$*;Trp53*$^{F/F}$ (KB1P) mice were a gift from Dr. Jos Jonkers (Netherlands Cancer Institute). KB1P mice were maintained on FVB/nJ background and generation of this strain has previously been described, where a human K14 gene promoter drives *Cre* recombinase transgene expression, resulting in LoxP *Trp53*- and *Brca1*-specific deletion in the mammary epithelium [31]. This genetically engineered mouse model resembles human triple negative breast cancer and mice develop single mammary tumors at approximately 25–30 weeks of age. *Cre* recombinase negative (*Cre*$^{-}$) female littermates were used as wild-type (WT) controls. Mice were palpated twice per week from 12 weeks of age for mammary tumors and perpendicular tumor diameters were measured with a caliper. Mice were sacrificed once a tumor reached >1 cm in any direction.

Mice were bred and maintained in the animal facility at Imperial College London (London, UK) or the Cancer Research Beatson Institute (Glasgow, UK) in a specific pathogen-free environment. Work was carried out in compliance with the British Home Office Animals Scientific Procedures Act 1986 and the EU Directive 2010 and sanctioned by Local Ethical Review Process (PPL 70/8606 and 70/8645). The animal research adhered to the ARRIVE guidelines.

Blockade of NKG2D *in vivo*

Female FVB/n mice at 8–10 weeks old (purchased from Charles River) were orthotopically transplanted in their mammary fat pat with 1 × 1 mm tumor pieces from syngeneic *K14-Cre;Brca1*$^{F/F}$*;Trp53*$^{F/F}$ (KB1P) mice. Once tumors reached 1 cm, animals were injected intraperitoneally with a single dose of 200 µg anti-NKG2D (Clone HMG2D, BioXCell) on day 1 followed by individual injections of 100 µg on two consecutive days. Control mice followed the same dosage regime with Armenian hamster IgG isotype control (Clone Polyclonal, Bio X Cell). Tumor growth was measured by calipers and mice were euthanized 1 day after final antibody injection.

Tissue processing

Tumors isolated from KB1P mice were collected in PBS, cut into small pieces, and resuspended in Dulbecco's Modified Eagle Medium F12 (DMEM) containing 30% fetal calf serum (FCS) and 10% dimethyl sulfoxide and stored at −150°C. Lungs, lymph nodes (LN) (axillary, brachial, mesenteric), and/or the spleen were isolated in ice-cold phosphate-buffered saline (PBS). Lungs were mechanically dissociated by using a scalpel and transferred to collagenase solution consisting of DMEM supplemented with collagenase D (Roche, 1 mg/ml) and DNaseI (ThermoFisher, 25 µg/ml). Enzymatic dissociation was assisted by heat and mechanical tissue dissociation, using the gentleMACS Octo Dissociator (Miltenyi Biotec) (run name: 37C_m_LDK), according to the manufacturer's dissociation protocol. The lung cell suspension was filtered through a 70-µm cell strainer using a syringe plunger and enzyme activity was stopped by addition of 2 ml of FCS followed by 5 ml of DMEM medium supplemented with 10% FCS, l-glutamine (2 mM, ThermoFisher) and penicillin (10 000 U/ml)/ streptomycin (10 000 µg/ml, ThermoFisher). Spleen and LN were processed and filtered through a 70-µm cell strainer using a syringe plunger, and the tissue was flushed through with PBS containing 0.5% bovine serum albumin (BSA). Cell suspension were centrifuged at 201 × *g* for 5 min, and supernatant was discarded. Cells were resuspended in PBS containing 0.5% BSA and cell number was determined using a hemocytometer.

The small intestine (SI) and tumor from control mice (age-matched *Villin-Cre*^{ERT2} negative;*Apc*$^{F/+}$ mice) and *Villin-Cre*^{ERT2};*Apc*$^{F/+}$ mice were collected in PBS, cut into small pieces using a McIlwain tissue chopper (Campden Instruments Ltd), and digested by heat and mechanical tissue dissociation using the gentleMACS Octo Dissociator (Miltenyi Biotec) (run name: 37C_m_TDK_1), according to the manufacturer's dissociation protocol. Cells were resuspended in PBS containing 0.5% BSA.

Small intestine and colon were harvested from healthy *Klrk1*$^{+/+}$, *Klrk1*$^{-/-}$, and *Apc*$^{min/+}$ mice. Once the cecum was removed, the small intestine was separated into duodenum, jejunum, and ileum. Data presented in this study relate to tumors isolated from the ileum unless otherwise stated. Remaining fat, as well as the gut content, was removed from the intestine before it was flushed with PBS. For tumor cell isolation, the tumor was carefully excised avoiding cutting through tumors. Mucus was removed, and tumor cells were counted before they were carefully removed from the intestinal tissue and minced using a scalpel. Tissue was transferred to a 1.5 ml tube and 1 ml of RPMI-1640 containing 5% FCS, 25 mM HEPES, 150 U/ml collagenase IV (Sigma–Aldrich), and 50 U/ml DNase (Roche) were added. Tubes were shaken in a horizontal position on an incubator shaker (37°C, 200 rpm, 30 min). Dissociated tissue was transferred to a 50 ml tube through a 100 µm cell strainer. To further dissociate the tissue, it was pushed through the filter using the plunger of a 2 ml syringe. To inhibit enzyme activity, 1 ml of PBS containing 10% FCS and 5 mM EDTA was added to the 1.5 ml tube and then transferred to the 50 ml tube. Cells were centrifuged for 10 minutes at 500 × g and resuspended in RPMI-1640 containing 5% FCS.

To isolate intraepithelial lymphocytes, the tissue was cut into small pieces and transferred to a 15 ml tube containing 10 ml of HBSS containing 1 mM DTT, 2% FCS, 100 U/ml penicillin, and 100 µg/ml streptomycin. Tubes were vortexed for 30 s and the solution was replaced. Tubes were shaken in a horizontal position on an incubator shaker (37°C, 200 rpm, 20 min), which resulted in the removal of the mucus layer. Using a 100 µm cell strainer, the tissue was then transferred to a new 15 ml tube containing 10 ml of HBSS containing 1 mM EDTA, 2% FCS, 100 U/ml penicillin, and 100 µg/ml streptomycin. It was again shaken in a horizontal position (37°C, 200 rpm, 15 min), before it was filtered through a 100 µm strainer. The liquid was taken up and the tissue transferred back to the 15 ml tube and 10 ml of fresh solution was added. This step was repeated two or three times for large and small intestine, respectively, and resulted in the removal of all epithelial cells. This resulted in a single cell suspension, which was then centrifuged for 10 min at 500 × *g* and resuspended in RPMI-1640 containing 5% FCS.

Magnetic-activated cell sorting to isolate T cells

To isolate T cells from lung, LN and spleen, single-cell suspensions were obtained as previously described. $CD3^+$ cell enrichment was achieved by MojoSort negative selection using MojoSort mouse $CD3^+$ T-cell Isolation Kit (BioLegend) according to manufacturer's instructions. In brief, 1×10^7 cells were resuspended in 100 µl MojoSort buffer and cells were incubated with 10 µl of the biotin-antibody cocktail in a 5-ml polypropylene tube and incubated for 15 min on ice. Streptavidin nanobeads (10 µl) were added and mixed, and incubated on ice for further 15 min. MojoSort buffer (2.5 ml) was added and the tube placed in the magnet for 5 min to allow magnetically labeled cells to bind to the tube and magnetic separator. The untouched $CD3^+$ cells were collected by decanting the liquid into a new tube. Cells after enrichment were counted with a hemocytometer and plated at a density of 1×10^6 cells/ml in round bottom 96-well plates.

Cell culture

YAC-1 lymphoma cells were maintained in RPMI-1640 medium supplemented with 10% FCS, 100 U/ml penicillin and streptomycin, and 2 mM glutamine and kept in incubators at 37°C under normoxic conditions. Freshly isolated T cells were added at an effector: target (E:T) ratio of 10:1 to YAC-1 cells. Co-cultures were incubated in normoxia at 20% O_2, 5% CO_2, and 37 °C for 48 h in complete IMDM medium (supplemented with 10% FCS, l-glutamine (2 mM) and penicillin (10 000 U/ml) and streptomycin (10000 µg/ml) and 50 µM *b*-mercaptoethanol).

Flow cytometry

Prior to antibody staining, cells were stimulated with PMA (final concentration 600 ng/ml), ionomycin (final concentration 100 ng/ml), and Brefeldin A (final concentration 10 µg/ml) in RPMI-1640 containing 5% FCS, 100 U/ml penicillin, and 100 µg/ml streptomycin to enhance cytokine production. Unspecific binding by the Fc receptor was prevented by incubation of anti-mouse CD16+CD32 (BD) for 20 min. Dead cells were stained using the LIVE/DEAD Fixable Aqua Dead Cell Stain kit (ThermoFisher) or the Zombie NIR Fixable Viability Dye (BioLegend) before antibodies were added and incubated for 30 minutes. Before staining of intracellular cytokines and transcription factors, cells were permeabilized using the Transcription Factor Fixation/Permeabilization kit (eBioscience). Antibodies to detect intracellular antigens were added and incubated for 30 min before cells were washed and transferred to round-bottom polystyrene 5 ml tubes through a filter mesh. Samples were acquired on a BD LSR Fortessa and analyzed using FlowJo software. All antibodies used in this study are listed in Supplementary Table 1.

Immunohistochemistry

Swiss rolls of intestines were prepared according to published protocols [50]. Tissues were fixed in 10% formalin in water overnight and then transferred to 70% ethanol where it was kept until paraffin embedding. Paraffin blocks were cut into 4 µm sections using a microtome (Leica), placed in a 40°C water bath, and affixed onto Superfrost Plus Microscope Slides (Thermo Scientific). Prior to staining, slides were deparaffinized and rehydrated. After heat-induced epitope retrieval (HIER), several blocking steps were performed to prevent nonspecific binding of antibodies. Primary antibody [anti-mouse RAE-1 pan-specific antibody, recognizing RAE-1α, -β, -δ, -γ, and -ε (R&D Systems, Catalogue Number AF1136)] or an appropriate isotype-matched control (polyclonal goat isotype IgG, NEB) was added at a final concentration of 10 µg/ml and incubated overnight. After several washing steps, the secondary antibody (10 µg/ml of biotinylatd rabbit anti-goat, Vectorlabs) was added and incubated for 30 min. The antigen was revealed using ABC (Vectorlabs) and DAB reagents (Abcam). Slides were counterstained by immersion in Harris Haematoxylin and dehydrated before coverslips were mounted using HistoMount mounting medium (ThermoFisher). Slides were scanned using an AxioScan.Z1 slide scanner (Zeiss). For image analysis, tumors and surrounding tissue were identified and marked using Fiji software (ImageJ). Percentage of positive cells was determined using a macro by comparing specific stained samples to isotype-matched Ig control samples.

Statistical analysis

Statistical analysis was performed using Python, Pandas, or GraphPad Prism. Shapiro-Wilk tests were performed to test for normality and significance was determined using Mann–Whitey U or unpaired *t* tests. For comparison on multiple groups, one-way ANOVA and Tukey's multiple comparison or Kruksal–Wallis and Dunn's multiple comparison were used following Shapiro–Wilk tests for normal distribution. Statistical significance of survival was determined using log-rank (Mantel–Cox) tests. Statistical significance of correlation analyses was determined using linear regression. Paired *t*-tests were performed when two variables of the same sample were compared. Data visualization was performed using GraphPad Prism (version 8.4.2).

Supplementary data

Supplementary data is available at *Discovery Immunology* online.

Acknowledgements

We thank S. Sheppard, P. Guermonprez, J. Helft, and G. Gorkiewicz for critical reading of the manuscript, B. Polić for providing reagents and insightful discussion, Adrian Hayday for providing reagents, J. Srivastava and J. Rowley from the Imperial College Flow Facility, L. Lawrence from the Imperial College Research Histology Facility, and the Blizard Core Pathology Facility for technical support. We thank the Core Services and Advanced Technologies at the Cancer Research UK Beatson Institute (C596/A17196), with particular thanks to the Biological Services and Flow Cytometry Facilities. The Editor-in-Chief, Simon Milling, and handling editor, Awen Gallimore, would like to thank the following reviewer, Matthias Eberl, and an anonymous reviewer, for their contribution to the publication of this article.

Funding

This work was supported by the Wellcome Trust RCDF (RCDF088381/Z/09/Z to N.G.), a Wellcome Trust PhD studentship (203948/Z/16A to S.C.), the Stevenson Fund to S.C., Breast Cancer Now (2018JulPR1101 to S.B.C.), Cancer Research UK Glasgow Centre (A25142 to S.B.C.), Wellcome Trust (208990/Z/17/Z to S.B.C.), Marie Curie

European Fellowship (GDCOLCA 800112 to T.S.) and Naito Foundation Grant for Research Abroad (to T.S).

Conflicts of interest

The authors declare no competing interests

Author contributions

S.C. designed and performed experiments, analyzed data and wrote the manuscript. S.C.E and T.S. designed and performed experiments, analyzed data and reviewed the manuscript. J.M., C.T. and N.Y. performed experiments and analyzed data. G.J., T.G. and D.R. contributed to some of the experiments. R.P. supervised the microbiota study. N.G. and S.B.C. designed and supervised the studies, analyzed the data and wrote the manuscript.

Ethical approval

The animal research here adhered to the ARRIVE guidelines (https://arriveguidelines.org/arrive-guidelines). Work was carried out in compliance with the British Home Office Animals Scientific Procedures Act 1986 and the EU Directive 2010 and sanctioned by Local Ethical Review Process (PPL 70/8606 and 70/8645).

Data availability

The authors declare that data will be made available upon request.

References

1. Sung H, Ferlay J, Siegel RL, et al. Global Cancer Statistics 2020: GLOBOCAN estimates of incidence and mortality worldwide for 36 cancers in 185 countries. *Ca Cancer J Clin* 2021, 71, 209–49. doi:10.3322/caac.21660.
2. Silva-Santos B, Mensurado S, Coffelt SB. γδ T cells: pleiotropic immune effectors with therapeutic potential in cancer. *Nat Rev Cancer* 2019, 19, 392–404. doi:10.1038/s41568-019-0153-5.
3. Shen L, Huang D, Qaqish A, et al. Fast-acting γδ T-cell subpopulation and protective immunity against infections. *Immunol Rev* 2020, 298, 254–63. doi:10.1111/imr.12927.
4. Girardi M, Oppenheim DE, Steele CR, et al. Regulation of cutaneous malignancy by γδ T cells. *Science* 2001, 294, 605–9. doi:10.1126/science.1063916.
5. Strid J, Roberts SJ, Filler RB, et al. Acute upregulation of an NKG2D ligand promotes rapid reorganization of a local immune compartment with pleiotropic effects on carcinogenesis. *Nat Immunol* 2008, 9, 146–54. doi:10.1038/ni1556.
6. Coffelt SB, Kersten K, Doornebal CW, et al. IL-17-producing γδ T cells and neutrophils conspire to promote breast cancer metastasis. *Nature* 2015, 522, 345–8. doi:10.1038/nature14282.
7. Wellenstein MD, Coffelt SB, Duits DEM, et al. Loss of p53 triggers WNT-dependent systemic inflammation to drive breast cancer metastasis. *Nature* 2019, 572, 538–42. doi:10.1038/s41586-019-1450-6.
8. Jin C, Lagoudas GK, Zhao C, et al. Commensal microbiota promote lung cancer development via γδ T cells. *Cell* 2019, 176, 998–1013.e16. doi:10.1016/j.cell.2018.12.040.
9. Marsh L, Coletta PL, Hull MA, et al. Altered intestinal epithelium-associated lymphocyte repertoires and function in ApcMin/+ mice. *Int J Oncol* 2012, 40, 243–50. doi:10.3892/ijo.2011.1176.
10. Housseau F, Wu S, Wick EC, et al. Redundant innate and adaptive sources of IL17 production drive colon tumorigenesis. *Cancer Res* 2016, 76, 2115–24. doi:10.1158/0008-5472.CAN-15-0749.
11. Lanier LL. NKG2D receptor and its ligands in host defense. *Cancer Immunol Res* 2015, 3, 575–82. doi:10.1158/2326-6066.CIR-15-0098.
12. Spits H, Bernink JH, Lanier L. NK cells and type 1 innate lymphoid cells: partners in host defense. *Nat Immunol* 2016, 17, 758–64. doi:10.1038/ni.3482.
13. Guerra N, Lanier LL. Editorial: Emerging concepts on the NKG2D receptor-ligand axis in health and diseases. *Front Immunol* 2020, 11, 562. doi:10.3389/fimmu.2020.00562.
14. Diefenbach A, Jensen ER, Jamieson AM, et al. Rae1 and H60 ligands of the NKG2D receptor stimulate tumour immunity. *Nature* 2001, 413, 165–71. doi:10.1038/35093109.
15. Guerra N, Tan YX, Joncker NT, et al. NKG2D-deficient mice are defective in tumor surveillance in models of spontaneous malignancy. *Immunity* 2008, 28, 571–80. doi:10.1016/j.immuni.2008.02.016.
16. Cerwenka A, Baron JL, Lanier LL. Ectopic expression of retinoic acid early inducible-1 gene (RAE-1) permits natural killer cell-mediated rejection of a MHC class I-bearing tumor in vivo. *Proc Natl Acad Sci USA* 2001, 98, 11521–6.
17. Baumeister SH, Murad J, Werner L, et al. Phase 1 trial of autologous CAR T cells targeting NKG2D ligands in patients with AML/MDS and multiple myeloma. *Cancer Immunol Res* 2019, 7, 100–12. doi:10.1158/2326-6066.CIR-18-0307.
18. Xiao L, Cen D, Gan H, et al. Adoptive transfer of NKG2D CAR mRNA-engineered natural killer cells in colorectal cancer patients. *Mol Ther* 2019, 27, 1114–25. doi:10.1016/j.ymthe.2019.03.011.
19. Curio S, Jonsson G, Marinovic S, et al. A summary of current NKG2D-based CAR clinical trials. *Immunother Adv* 2021, 1. doi:10.1093/immadv/ltab018.
20. Allez M, Tieng V, Nakazawa A, et al. CD4+NKG2D+ T cells in Crohn's disease mediate inflammatory and cytotoxic responses through MICA interactions. *Gastroenterology* 2007, 132, 2346–58. doi:10.1053/j.gastro.2007.03.025.
21. Meresse B, Chen Z, Ciszewski C, et al. Coordinated induction by IL15 of a TCR-independent NKG2D signaling pathway converts CTL into lymphokine-activated killer cells in celiac disease. *Immunity* 2004, 21, 357–66. doi:10.1016/j.immuni.2004.06.020.
22. Farhadi N, Lambert L, Triulzi C, et al. Natural killer cell NKG2D and granzyme B are critical for allergic pulmonary inflammation. *J Allergy Clin Immun* 2014, 133, 827–835.e3.
23. Sheppard S, Guedes J, Mroz A, et al. The immunoreceptor NKG2D promotes tumour growth in a model of hepatocellular carcinoma. *Nat Commun* 2017, 8, 13930. doi:10.1038/ncomms13930.
24. Sheppard S, Ferry A, Guedes J, et al. The paradoxical role of NKG2D in cancer immunity. *Front Immunol* 2018, 9, 1808. doi:10.3389/fimmu.2018.01808.
25. Grivennikov SI, Wang K, Mucida D, et al. Adenoma-linked barrier defects and microbial products drive IL-23/IL-17-mediated tumour growth. *Nature* 2012, 491, 254–8. doi:10.1038/nature11465.
26. Edwards SC, Hedley A, Hoevenaar WHM, et al. Single-cell analysis uncovers differential regulation of lung γδ T cell subsets by the co-inhibitory molecules, PD-1 and TIM-3. *BioRxiv* 2021. Doi:10.1101/2021.07.04.451035, preprint: not peer reviewed.
27. Groh V, Bahram S, Bauer S, et al. Cell stress-regulated human major histocompatibility complex class I gene expressed in gastrointestinal epithelium. *Proc Natl Acad Sci USA* 1996, 93, 12445–50.
28. Tan L, Sandrock I, Odak I, et al. Single-cell transcriptomics identifies the adaptation of Scart1+ Vγ6+ T cells to skin residency as activated effector cells. *Cell Reports* 2019, 27, 3657–3671.e4. doi:10.1016/j.celrep.2019.05.064.
29. Monin L, Ushakov DS, Arnesen H, et al. γδ T cells compose a developmentally regulated intrauterine population and protect against vaginal candidiasis. *Mucosal Immunol* 2020, 13, 969–81. doi:10.1038/s41385-020-0305-7.
30. Chae W-J, Gibson TF, Zelterman D, et al. Ablation of IL-17A abrogates progression of spontaneous intestinal tumorigenesis. *Proc Natl Acad Sci USA* 2010, 107, 5540–4.
31. Liu X, Holstege H, van der Gulden H, et al. Somatic loss of BRCA1 and p53 in mice induces mammary tumors with features of human

BRCA1-mutated basal-like breast cancer. *Proc Natl Acad Sci USA* 2007, 104, 12111–6.
32. Markiewicz MA, Wise EL, Buchwald ZS, et al. RAE1ε ligand expressed on pancreatic islets recruits NKG2D receptor-expressing cytotoxic T cells independent of T cell receptor recognition. *Immunity* 2012, 36, 132–41. doi:10.1016/j.immuni.2011.11.014.
33. Espinoza I, Agarwal S, Sakiyama M, et al. Expression of MHC class I polypeptide-related sequence A (MICA) in colorectal cancer. *Front Biosci (Landmark Ed)* 2021, 26, 765.
34. McGilvray RW, Eagle RA, Watson NFS, et al. NKG2D ligand expression in human colorectal cancer reveals associations with prognosis and evidence for immunoediting. *Clin Cancer Res* 2009, 15, 6993–7002. doi:10.1158/1078-0432.CCR-09-0991.
35. Zhao Y, Chen N, Yu Y, et al. Prognostic value of MICA/B in cancers: a systematic review and meta-analysis. *Oncotarget* 2017, 8, 96384–95. doi:10.18632/oncotarget.21466.
36. Deng W, Gowen BG, Zhang L, et al. Antitumor immunity. A shed NKG2D ligand that promotes natural killer cell activation and tumor rejection. *Science* 2015, 348, 136–9. doi:10.1126/science.1258867.
37. de Andrade LF, Tay RE, Pan D, et al. Antibody-mediated inhibition of MICA and MICB shedding promotes NK cell–driven tumor immunity. *Science* 2018, 359, 1537–42.
38. Tosolini M, Kirilovsky A, Mlecnik B, et al. Clinical impact of different classes of infiltrating T cytotoxic and helper cells (Th1, th2, treg, th17) in patients with colorectal cancer. *Cancer Res* 2011, 71, 1263–71. doi:10.1158/0008-5472.CAN-10-2907.
39. Wu P, Wu D, Ni C, et al. γδT17 cells promote the accumulation and expansion of myeloid-derived suppressor cells in human colorectal cancer. *Immunity* 2014, 40, 785–800. doi:10.1016/j.immuni.2014.03.013.
40. Babic M, Dimitropoulos C, Hammer Q, et al. NK cell receptor NKG2D enforces proinflammatory features and pathogenicity of Th1 and Th17 cells. *J Exp Med* 2020, 217, e20190133.
41. Wakita D, Sumida K, Iwakura Y, et al. Tumor-infiltrating IL-17-producing γδ T cells support the progression of tumor by promoting angiogenesis. *Eur J Immunol* 2010, 40, 1927–37. doi:10.1002/eji.200940157.
42. Tang Q, Li J, Zhu H, et al. Hmgb1-IL-23-IL-17-IL-6-Stat3 axis promotes tumor growth in murine models of melanoma. *Mediators Inflamm* 2013, 2013, 1–13.
43. Lonez C, Hendlisz A, Shaza L, et al. Celyad's novel CAR T-cell therapy for solid malignancies. *Curr Res Transl Med* 2018, 66, 53–6.
44. Murad JM, Baumeister SH, Werner L, et al. Manufacturing development and clinical production of NKG2D chimeric antigen receptor–expressing T cells for autologous adoptive cell therapy. *Cytotherapy* 2018, 20, 952–63. doi:10.1016/j.jcyt.2018.05.001.
45. Lu S, Zhang J, Liu D, et al. Nonblocking monoclonal antibody targeting soluble MIC revamps endogenous innate and adaptive antitumor responses and eliminates primary and metastatic tumors. *Clin Cancer Res* 2015, 21, 4819–30.
46. Vadstrup K, Bendtsen F. Anti-NKG2D mAb: a new treatment for Crohn's disease? *Int J Mol Sci* 2017, 18, 1997.
47. Marjou FE, Janssen K, Chang BH, et al. Tissue-specific and inducible Cre-mediated recombination in the gut epithelium. *Genesis* 2004, 39, 186–93.
48. Shibata H, Toyama K, Shioya H, et al. Rapid colorectal adenoma formation initiated by conditional targeting of the *Apc* gene. *Science* 1997, 278, 120–3. doi:10.1126/science.278.5335.120.
49. Itohara S, Mombaerts P, Lafaille J, et al. T cell receptor δ gene mutant mice: independent generation of αβ T cells and programmed rearrangements of γδ TCR genes. *Cell* 1993, 72, 337–48. doi:10.1016/0092-8674(93)90112-4.
50. Bialkowska AB, Ghaleb AM, Nandan MO, et al. Improved Swiss-rolling technique for intestinal tissue preparation for immunohistochemical and immunofluorescent analyses. *J Vis Exp* 2016, 4161, e54161–e5.